Structural Characterization of Ionic Gelator Studied by Dynamic Light Scattering and Small-Angle Neutron Scattering

ARTICLE *in* THE JOURNAL OF PHYSICAL CHEMISTRY B · JANUARY 2009

Impact Factor: 3.3 · DOI: 10.1021/jp807992t · Source: PubMed

Article

Structural Characterization of Ionic Gelator Studied by Dynamic Light Scattering and Small-Angle Neutron Scattering

Shyamal Kumar Kundu, Noboru Osaka, Takuro Matsunaga, Masaru Yoshida, and Mitsuhiro Shibayama

J. Phys. Chem. B, **2008**, 112 (51), 16469-16477 • DOI: 10.1021/jp807992t • Publication Date (Web): 02 December 2008

Structural Characterization of Ionic Gelator Studied by Dynamic Light Scattering and Small-Angle Neutron Scattering

Shyamal Kumar Kundu, Noboru Osaka, Takuro Matsunaga, Masaru Yoshida,† and Mitsuhiro Shibayama*

Institute for Solid State Physics, The University of Tokyo, 5-1-5 Kashiwanoha, Kashiwa, Chiba 277-8581, Japan, and Nanotechnology Research Institute, National Institute of Advanced Industrial Science and Technology (AIST), 1-1-1 Higashi, Tsukuba, Ibaraki 305-8565, Japan

Received: September 9, 2008; Revised Manuscript Received: October 29, 2008

Structural characterization of a hydrogel consisting of an oligomeric electrolyte, poly[pyridinium-1,4-diyliminocarbonyl-1,4-phenylenemethylene chloride] (**1-Cl**) as an ionic gelator was carried out by static and dynamic light scattering (SLS/DLS) and small-angle neutron scattering (SANS) techniques. All the measurements were performed by changing the concentration and temperature. We have successfully obtained the weight average molecular weight and the degree of polymerization of poly(**1-Cl**) by SLS. The sol−gel transition was clearly observed as large fluctuations in the scattering intensity of the time−intensity correlation function. Time correlation function of the scattering light intensity entailed a power law behavior at the sol−gel transition. **1-Cl** hydrogel showed strong hysteresis and its hysteresis loop was observed both by DLS and rheological methods. We have estimated the critical concentration of gelation and the gelation temperature by DLS. The enthalpy change for gelation was estimated to be ca. −10 kJ/mol. SANS experiments revealed that the unit structure of the gel network is responsible for the gelation of **1-Cl** hydrogel.

1. Introduction

Investigations of the physical properties of hydrogels with varying water contents have been acquired special significance, both from fundamental and application points of view.[1,2] A variety of organo- and hydrogelators capable of immobilizing organic fluids and/or water have been proposed, in which various types of intermolecular interactions, such as hydrogen (H)-bond, $\pi-\pi$, cation$-\pi$, and electrostatic interactions, play a significant role. These interactions bestow unique properties to polymer gels, which are readily applied to biological and pharmaceutical products and medical applications. The broad utility of gels has made the search for new gelators a very active area of science. Despite such efforts, our understanding of the formation of gels remains incomplete.

Although already in 1892 a low-molecular-weight (LMW) gelator was reported to be capable of gelating water,[3] the development of self-assembling LMW hydrogelators attracted considerable attention only in recent years, arising from the progress in the field of LMW organogelators as well as many applications that can be envisaged. Since then, different types of LMW gelators have been produced from those gels in which the molecules are self-assembled into a three-dimensional network, solely held together by noncovalent interactions. LMW gelators have emerged as an attractive alternative to the widely used polymeric gelators because of their rapid response toward external stimuli as well as thermoreversible nature.[4−11] The behavior of LMW gelators is a subject of special interest[4,12−19] because of their wide application including oil recovery.

In our previous report,[20] we studied an oligomeric electrolyte, poly[pyridinium-1,4-diyliminocarbonyl-1,4-phenylenemethylene chloride] (**1-Cl**) aqueous solutions, by rheology and discussed the gelation mechanism, gel healing, and the gel recovery process in detail. It was also shown that the **1-Cl** hydrogel recovered its elastic properties faster than other hydro- and organogels and the activation energy was estimated to be ca. −10 kJ/mol. As **1-Cl** hydrogel displayed remarkable properties, it behaves like a low molecular weight polymers. However, detailed characterization of the structure and dynamics of this novel hydrogel has not been done yet. It is needless to mention that scattering methods are powerful tools to explore the structure and dynamics of this gel.

The objective of the present study is to characterize the novel oligomeric electrolyte, **1-Cl**, by static/dynamic light scattering (SLS/DLS) and small-angle neutron scattering (SANS). We will examine both the network formation and the gel structure using SLS/DLS and SANS. We will discuss the sol−gel transition and the hysteresis behavior of **1-Cl** by DLS. We will estimate the weight average molecular weight, radius of gyration, and hydrodynamic radius of **1-Cl** in dilute aqueous solutions using SLS/DLS. It is also possible to obtain the critical concentration of gelation and threshold gelation temperature by DLS.

2. Experimental Section

2.1. Sample. A novel oligomeric electrolyte, **1-Cl**, was prepared in a similar manner to the previous report.[21] A powder of **1-Cl** was immersed in distilled water, and the mixture was sonicated for 30 min. Then, the dispersion was heated at around 97 °C by a heat gun to form a clear isotropic sol phase (**1-Cl**/water). The concentrations of 0.1−20 g/L **1-Cl** were used for SLS/DLS and SANS measurements.

2.2. Static and Dynamic Light Scattering (SLS/DLS). SLS/DLS experiments were carried out by ALV-5000-F SLS/DLS compact goniometer system (Langen, Germany). A He−Ne laser with the wavelength of 632.8 nm was used as incident beam. The scattered photons were collected with an avalanche photodiode system, and the scattered intensity was obtained as the

* To whom correspondence should be addressed. E-mail: sibayama@issp.u-tokyo.ac.jp.
† National Institute of Advanced Industrial Science and Technology.

10.1021/jp807992t CCC: $40.75
Published on Web 12/02/2008

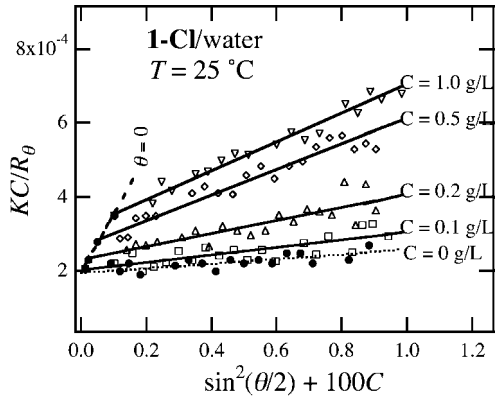

Figure 1. Zimm plot for **1-Cl**/water at 25 °C.

counting rate of the photons. In SLS, the intensity of the scattered light from the solvent (water) and the solutions (**1-Cl**/water mixtures) was measured at different scattering angles, θ, in the range of 30°−150° at 25 °C. The specific refractive index increment, dn/dC, of **1-Cl** in pure water was measured using a double-beam differential refractometer (Otsuka Electronics, DRM-1021) at 25 °C. The value of dn/dC was 0.284 ± 0.005 mL/g.

In DLS, the time−intensity correlation function (ICF) was calculated as a convolution of the scattered intensity. The typical measuring time was 30 s, and the scattering angle was 90°. For the sake of determining the gelation points, the scattered light intensity was monitored as a function of temperature. The temperature of the sample was carefully controlled with a water circulating system (RTE-111M, Neslab, Co., Ltd., Newton, MA). For observation of the gelation and the gel melting temperatures, the experiments were performed by heating and cooling processes with a rate of 0.12 °C/min. Time-dependent DLS measurements were done by temperature jump method. The gelation time was observed at 25 °C. Note that the temperature was fixed during measurements with the precision of 0.1 °C.

2.3. Small-Angle Neutron Scattering (SANS). SANS experiments were carried out at the SANS-U spectrometer (The University of Tokyo, Tokai, Japan). The wavelength of the incident neutron beam was 0.7 nm. Scattered neutrons were collected with an area detector of 64 cm × 64 cm (Ordela, 2660N). The samples were loaded in quartz cells with the thickness of 1 mm for 10 g/L and 20 g/L **1-Cl** samples and 2 mm for 5 g/L, 7.5 g/L and 8.5 g/L **1-Cl** samples. A standard data reduction such as subtraction of the cell scattering and division by the sample thickness was carried out. The scattered intensity was scaled to the absolute intensity with the incoherent scattering from a polyethylene secondary standard sample, and then subtraction of the incoherent scattering from the solute and the solvent was performed. The temperature of the samples was controlled with a Neslab, RTE-111 and a programmable heating system with a stability of 0.01 °C.

3. Result and Discussion

3.1. Static Light Scattering (SLS). The scattering light intensity of **1-Cl** in dilute aqueous solutions was measured by a laser light scattering instrument mentioned above. The angular and the concentration dependences of scattered intensities were analyzed by standard (Zimm) analysis. The scattering intensity from solutions is expressed as

$$\frac{KC}{R_\theta} = \frac{1}{M_w}\left(1 + \frac{16\pi^2 n'^2 R_g^{\,2}}{3\lambda^2}\sin^2\frac{\theta}{2}\right) + 2A_2C \qquad (1)$$

where M_w is the weight average molecular weight, R_g is the radius of gyration, A_2 is the second virial coefficient, λ is the wavelength of the incident light, n' is the refractive index of the solvent, and K is the optical constant which is

$$K = \frac{2\pi^2 n'^2 (dn'/dC)^2}{N_A \lambda^4} \qquad (2)$$

where C, dn'/dC, and N_A are respectively the concentration, the refractive index increment, and Avogadro's number. R_θ is the Rayleigh ratio, where $R_\theta = \Psi I_{sc}(\theta)$, $I_{sc}(\theta)$ being the scattering intensity from solutions and θ the scattering angle. Ψ is defined as

$$\Psi = \frac{R_{90,water}}{I_{water}} \qquad (3)$$

where $R_{90,water}$ and I_{water} are respectively the Rayleigh ratio of the scattered light ($R_{90,water} = 4.9 \times 10^{-7}$ cm^{-1})[22] and the scattering intensity in water at 90°. Figure 1 shows the Zimm plot of KC/R_θ against $\sin^2(\theta/2) + kC$ with $k = 100$ at 25 °C. This figure shows that the intensity of the scattered light is strongly concentration dependent. It might be due to self-organization of the **1-Cl** molecules. We estimated M_w and R_g using eq 1 at $C = 0$ (dotted line); and M_w and A_2 using eq 1 at $\theta = 0$ (dashed line). The values of M_w, A_2, and R_g are evaluated to be 5.12×10^3 Da, 7.88×10^{-5} cm^3 mol/g^2, and 35.7 nm, respectively. The weight average degree of polymerization was calculated to be 22.

3.2. Dynamic Light Scattering (DLS). The time correlation function of the scattering light intensity, $g^{(2)}(\tau)$, was obtained from the normalized field correlation function $g^{(1)}(\tau)$ by

$$g^{(2)}(\tau) = \frac{\langle I(0)I(\tau)\rangle_T}{\langle I(0)\rangle_T^2} = B[1 + B'|g^{(1)}(\tau)|^2] \qquad (4)$$

where B and B' are respectively constants depending on the instrument optics and the sample. τ is the decay time and $\langle I(0)\rangle_T$ means the time-average scattering intensity at time $\tau = 0$. For a polydisperse system, the autocorrelation function is no longer a single exponential and can be written as

$$g^{(1)}(\tau) = \int G(\Gamma)\exp(-\Gamma\tau)\,d\Gamma \qquad (5)$$

where $\int G(\Gamma)\,d\Gamma = 1$ and Γ is the characteristic decay rate.

Figure 2a shows the time correlation function of the scattered light intensity, $g^{(2)}(\tau)$, vs decay time, τ, for different concentrations of **1-Cl**/water at 25 °C at $\theta = 90°$. Figure 2b shows the decay time distribution function, $G(\tau)$, vs τ obtained by CONTIN analysis of $g^{(2)}(\tau)$. This system showed single relaxation mode. Let us assign the relaxation mode in the following section.

Figure 3a shows the Γ vs q^2 plot for **1-Cl**/water at 25 °C. The scattering vector **q** is of the form

$$q = \frac{4\pi n_L}{\lambda} \sin(\theta/2) \quad (6)$$

For simplicity, we have assumed that the refractive index of the very dilute solution is nearly same with the solvent (n_L = 1.332). The plot of Γ vs q^2 shows linear relation and follows $\Gamma = Dq^2$, where D is the translational diffusion coefficient. The diffusion coefficient, D, obtained from Figure 3a for different concentrations, is shown in Figure 3b. The hydrodynamic radius, R_h, of the diffusing particles can be calculated from the Stokes−Einstein relationship

$$R_h = \frac{k_B T}{6\pi\eta D} \quad (7)$$

where η (=0.89 mPa·s) is the solvent viscosity, k_B is the Boltzmann constant, D is the translational diffusion coefficient, and T is the absolute temperature. The hydrodynamic radius, R_h, obtained from D is also shown in Figure 3b. The average diffusion coefficient, $\langle D \rangle_{av}$, and the average hydrodynamic radius, $\langle R_h \rangle_{av}$, are evaluated to be 1.10×10^{-11} m^2/s and 22.4 nm, respectively. Note that the observed values of R_g and R_h are very large compared to the observed value of M_w. It might be attributed to the large aggregation of the molecules due to presence of counterions in the solution. However, a dimensionless quantity, ρ (=R_g/R_h), which is a measure of polymer conformation in terms of branching density and/or intrinsic flexibility of the polymer chains[23,24] is estimated to be ≈1.59. This value indicates that the structure of the gel is a rodlike assembly.[25,26] For confirmation of such a structure, SANS experiments have been performed and the results are discussed in section 3.4.

3.3. Time-Resolved Dynamic Light Scattering (TRDLS). Sol−gel transition is defined as a point where connectivity correlation diverges. Shibayama et al.[27,28] proposed four methods of gel-point determination with dynamic light scattering, DLS. The gel point is determined as a point at which one of the following features is observed: (i) a large fluctuation and a drastic increase in the scattering intensity, (ii) a power-law behavior in ICF, (iii) a characteristic broadening in the distribution function obtained by inverse Laplace transform of ICF, or (iv) a depression of the initial amplitude of ICF. The applicability of these methods was confirmed for chemical gels, physical gels, gelators, and glass-forming systems.[29] In our present study, we will use the first two criteria for the gel-point determination.

Time-dependent gelation measurements were carried our by temperature jump experiments. This procedure was already reported by Hashimoto et al.[30] on time-resolved X-ray scattering. We should mention here that the characteristic time for thermal diffusion was detected to be 0.4 min. This value is much smaller than that required for structural changes in physical gels and can be neglected within experimental error in this work. Figure 4 shows the time course of ICFs for 10 g/L **1-Cl**/water at 25 °C. The characteristic features depending on the capability of gelation are seen in this figure. At the beginning, the ICF shows two exponential functions. The relaxations are assigned to be the collective diffusion mode and the stretched exponential mode. The transition from a stretched exponential behavior (i.e., up to t = 9.5 min) to a power-law behavior (t = 9.6 min) is clearly observed. It is possible to analyze ICF data theoretically, which are mentioned below.

In the sol state, the ICF consists of the translational diffusion mode and the stretched exponential mode, as written by[31−34]

$$g_T^{(2)}(\tau) - 1 \approx \sigma_I^2\{A \exp(-Dq^2\tau) + (1 - A) \exp[-(\tau/\tau_c)^{\beta}]\}^2 \quad (8)$$

where σ_I^2 is the initial amplitude of ICF, D is the translational diffusion coefficient, A is the fraction of the translational diffusion mode ($0 \le A \le 1$), τ_c is the characteristic time for the stretched exponential mode, and β is the stretched exponent. When approaching a sol−gel transition point, τ_c becomes dominant and ICF becomes a power-law function, which is characterized by the following function:[34]

$$g_T^{(2)}(\tau) - 1 \approx \sigma_I^2\{A \exp(-Dq^2\tau) + (1 - A)[1 + (\tau/\tau^*)]^{(n-1)/2}\}^2 \quad (9)$$

where τ^* is the characteristic time where the power law behavior appears and n is the fractal dimension of the scattered photon ($0 < n < 1$). This exponent is same as that obtained by mechanical dispersion.[35−37]

In Figure 4, the dashed curves are fitting curves using eq 8 and the experimental data points are well fitted with eq 8, indicating that the **1-Cl** sol indeed has two modes, i.e., the fast mode and the slow mode. The fitting parameters are obtained from each ICF. The fitting parameters are, e.g., $\sigma_I^2 = 0.88$, $D = 8.8 \times 10^{-11}$ m^2/s, $A = 0.245$, $\tau_c = 3.78$ ms, and $\beta = 0.49$ at time t = 6.4 min. The correlation length (or the mesh size) ξ can be estimated from D via $\xi = kT/6\pi\eta D$. ξ is obtained from D to be 2.78 nm. In addition, the stretched exponential mode is assigned to translational diffusion of finite clusters. By changing time, finite clusters become larger and larger and the ICF accompanies a long tail at a slower relaxation time. At t = 9.6 min, the tail becomes the longest and the ICF is successfully fitted with eq 9 as shown with the solid curve in the figure. The fitted parameters will be discussed later.

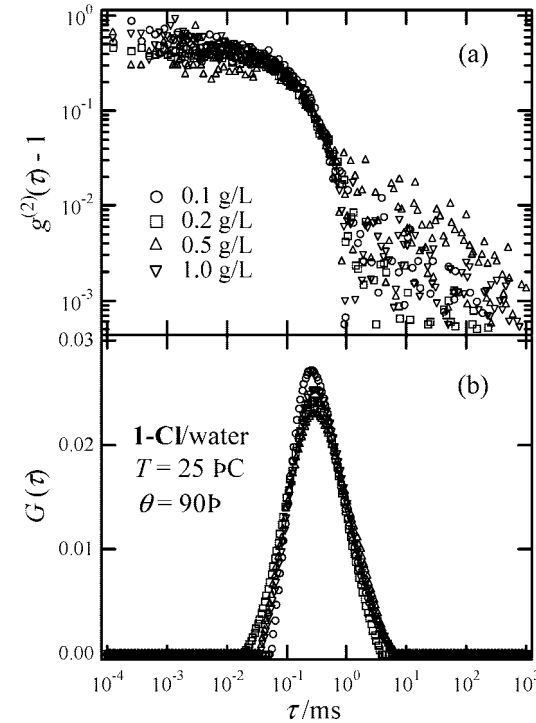

Figure 2. Variations of (a) time−intensity correlation function, $g^{(2)}(\tau)$, and (b) decay time distribution function, $G(\tau)$, vs decay time, τ, for **1-Cl**/water at 25 °C.

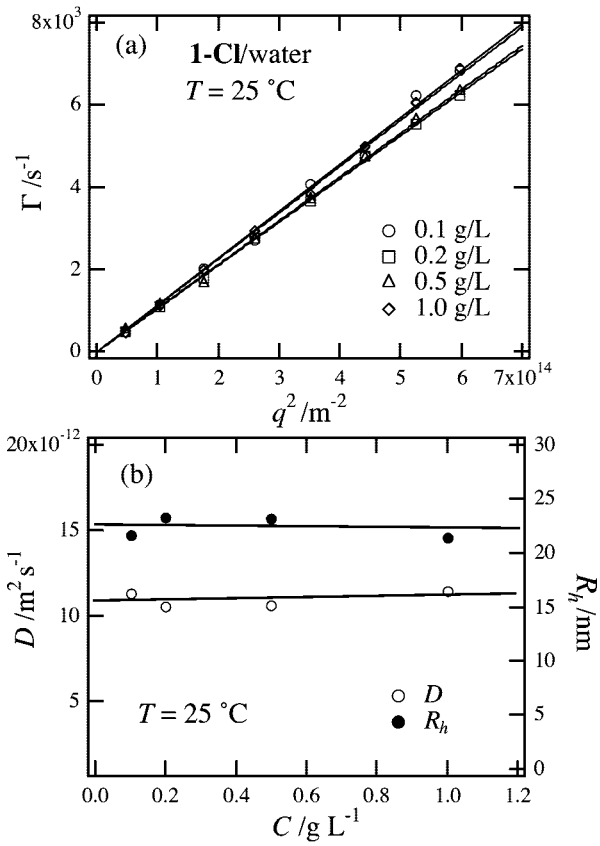

Figure 3. Variations of (a) decay rate, Γ, vs q^2 and (b) thermal diffusion, D, and the hydrodynamic radius, R_h, for **1-Cl**/water at 25 °C. The average diffusion coefficient $\langle D \rangle_{av}$ and the average hydrodynamic radius, $\langle R_h \rangle_{av}$, are evaluated to be 1.10×10^{-11} m^2/s and 22.4 nm, respectively.

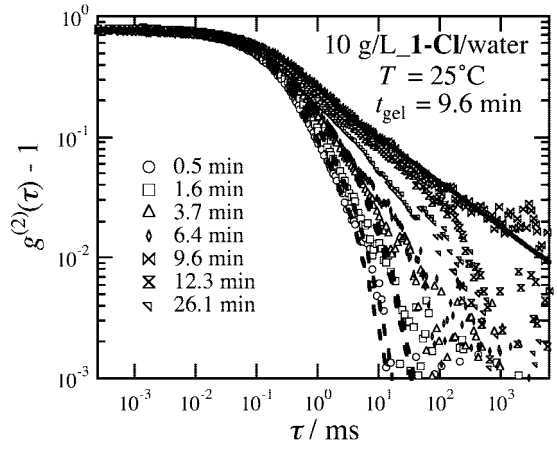

Figure 4. Time−intensity correlation function, $g^{(2)}(\tau)$, for 10 g/L **1-Cl**/water at 25 °C. The dashed curves are fitted curves with eq 8 and solid curve is fitted with eq 9.

On the other hand, the sol−gel transition was estimated by the large fluctuations of the scattering intensity. Figure 5 shows the variation of the intensity of the ICF with time for **1-Cl**/water at 25 °C. It is seen from this figure that at $t > 9.6$ min the intensity of the ICF strongly fluctuates with time. These fluctuations in the scattering intensity are ascribed to an emergence of nonergodicity[38] as the system becomes a gel.[39] Therefore, the gelation time obtained from the large fluctuations in the scattering intensity and a power-law behavior in ICF are observed to be at the same point, i.e., $t = 9.6$ min. Note that we have obtained the gelation time for different concentrations

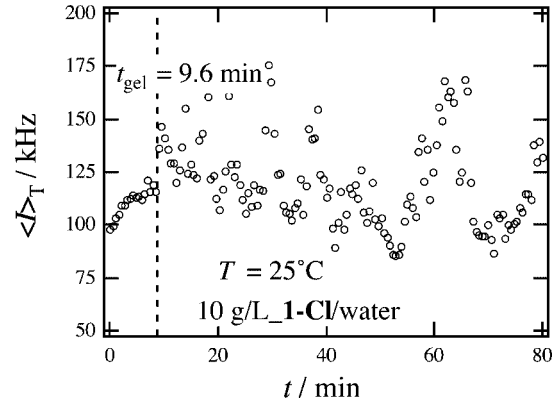

Figure 5. Variation of the scattering intensity with time for 10 g/L **1-Cl**/water at 25 °C.

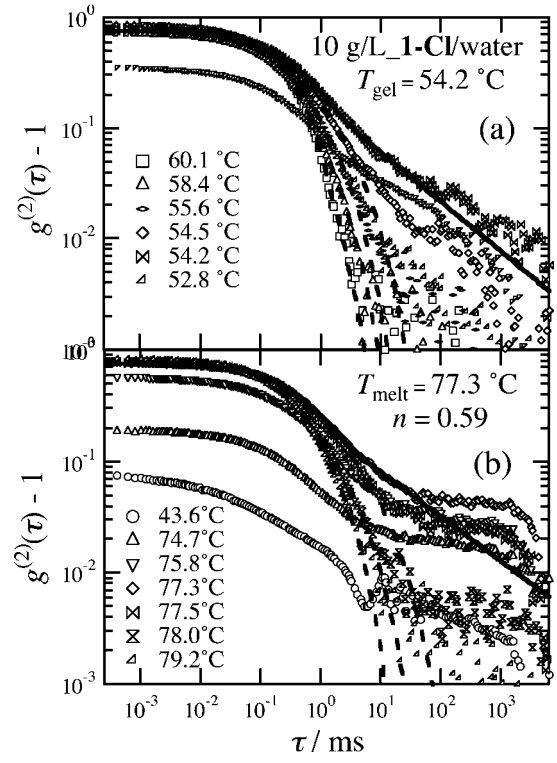

Figure 6. Time−intensity correlation function, $g^{(2)}(\tau)$, for 10 g/L **1-Cl**/water (a) during cooling and (b) during heating. The dashed curves are fitted curves with eq 8, and solid curves are fitted with eq 9.

in the same way as mentioned above and we will discuss only the concentration dependence of the gelation time later (Figures 9 and 10).

Temperature-dependent sol−gel transition measurements were carried out at constant cooling and heating rates. Figure 6, a and b, shows the temperature-dependent ICFs for during (a) cooling and (b) heating for 10 g/L **1-Cl**/water. The gelation and gel melting temperatures are well observed when ICF becomes a power-law function. At $T = 54.2$ °C (a gelation temperature) and at $T = 77.3$ °C (a gel melting temperature), the ICF tail becomes the longest and the ICF is successfully fitted with eq 9 as shown with the solid curves in the figures. The dashed curves in Figure 6a,b are the fitting curves using eq 8, indicating that the **1-Cl** sol indeed has two modes, i.e., the fast mode and the slow mode. The fitting parameters are well obtained for each ICF; e.g., at temperature $T = 58.4$ °C (during cooling), the fitting parameters are $\sigma_I^2 = 0.91$, $D = 7.40 \times 10^{-11}$ m^2/s, $A = 0.35$, $\tau_c = 1.3$ ms, and $\beta = 0.55$. The

correlation length ξ is obtained from D to be 3.3 nm. At temperature $T = 79.2$ °C (during heating), the fitting parameters are $\sigma_I^2 = 0.91$, $D = 7.90 \times 10^{-11}$ m^2/s, $A = 0.27$, $\tau_c = 1.98$ ms, and $\beta = 0.58$. The correlation length ξ is obtained from D to be 3.1 nm. The stretched exponential mode is assigned to translational diffusion of finite clusters. On the other hand, at the sol−gel transition, the fitting parameters are well obtained using eq 9.

The concentration dependences of some of the fitting parameters, e.g., τ^*, A, and n, obtained from eq 9 at the sol−gel transition are shown in Figure 7. This figure shows that τ^* and A are concentration-dependent irrespective of t_{gel}, T_{gel}, and T_{melt}. It is quite surprising that n is almost concentration independent and its value is $n \approx 0.6$. Winter[35] reported $n \approx 0.5$ for polydimethylsiloxane, Durand et al.[36] obtained $n \approx 0.73$ for branched polymer, and Matsunaga and Shibayama[37] obtained $n \approx 0.73$ for gelatin. Muthukumar[40] explained these variations in n in terms of hydrodynamic screening effect and excluded volume effect.

Figure 8 shows the variation of the scattering intensity with temperature during cooling and heating processes for 10 g/L **1-Cl**/water. The gelation and gel melting temperatures are easily obtained and are indicated by the dashed lines. As shown in this figure, **1-Cl** exhibited a large hysteresis loop during a temperature cycle. Hence, this system is thermally reversible. The gelation temperature, T_{gel}, during cooling process and the gel melting temperature, T_{melt}, during heating process for **1-Cl**/water were determined as the point where the scattering intensity starts fluctuations. The T_{gel} and T_{melt} are observed to be 54.2 and 77.3 °C, respectively. Similar results were obtained by rheological measurements[20] on this system. Therefore, one can say that the sol−gel transition points obtained by macroscopically and microscopically[37] are almost identical.

The concentration dependences of the gelation time (t_{gel}), gelation temperature (T_{gel}), and gel melting temperature (T_{melt}) are shown in Figure 9. This figure shows that T_{gel} and T_{melt} increase exponentially with increasing concentration of **1-Cl** and follow the relation $T_j = T_{\infty j} - A' \exp(-aC)$. Here, j = gel indicates gelation and j = melt indicates gel melting. A' and a are constants. $T_{\infty j}$ is the saturation value of T_j. The calculated values of $T_{\infty j}$ are respectively 88.7 °C (for gelation) and 90.1 °C (for gel melting). Therefore, the T_{gel} and T_{melt} are very close to each other, because they approach the gel preparation temperature. Figure 9 also shows that t_{gel} decreases sharply with increasing concentration.

Figure 10a shows the time (t_{gel})−temperature (T_{gel}) phase diagram on **1-Cl**/water mixtures. The experimental points are followed by the equation:

$$t_{gel} = a'(T_{gel} - T_c)^{-\alpha} \tag{10}$$

where a' is a constant, T_c is the threshold gelation temperature, and α is the power law exponent. The solid curve is the fitting curve with eq 10. The evaluated values of T_c and α are respectively 17.1 °C and 2.8. However, the value of α obtained from eq 10 could be close to the fractal dimension, D. Note that by taking account of hydrodynamic screening effects as discussed by Muthukumar[41] and Martin,[42] the fractal dimension is obtained to be $D \approx 3$ where the power law exponent $n \approx 0.6$ obtained from eq 9. We can also estimate the critical concentration of gelation from Figure 9, and this value is estimated to be 6.3 g/L at 17.1 °C. It should be mentioned here that the gelation threshold was estimated[43,44] from the ratio of the storage modulus

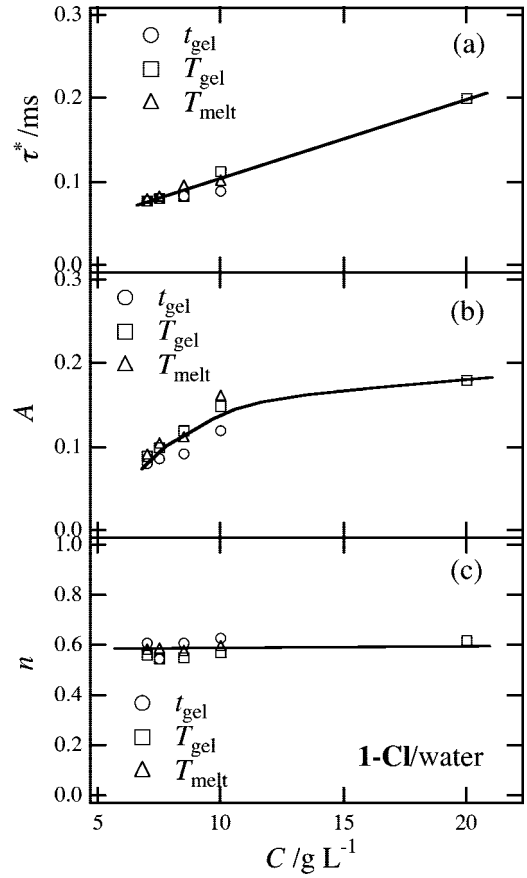

Figure 7. Variations of τ^*, A, and n obtained from eq 9 at the gelation and gel melting points with concentration, C. The solid lines are drawn as a guide for the eye.

(G') to loss modulus (G'') for different polypeptides as a function of concentration. The crossover point where $G' = G''$ provides the measure for the gelation threshold, making the transition from predominantly viscous to elastic properties. However, the DLS also provides an accurate measure for the gelation threshold.

As shown in Figure 9, it was found that T_{gel} and T_{melt} were dependent on **1-Cl** concentration. Figure 10b shows that dependence of the reciprocal gelation and gel-melting temperatures on ln C. The concentration dependence of T_{gel} and T_{melt} are well estimated from van't Hoff equation:

$$\ln C = \text{constant} + \frac{\Delta H_i}{RT_i} \tag{11}$$

where R is the gas constant, ΔH_i is the enthalpy of cross-link formation, and T_i is the absolute temperature. i = gel indicates gelation and i = melt indicates gel melting. The values of ΔH_i are evaluated to be $\Delta H_{gel} = -10.5 \pm 1.5$ kJ/mol $\Delta H_{melt} = -11.6 \pm 1.7$ kJ/mol. The negative sign indicates that the enthalpy of cross-link formation is an exothermic process. These values are almost the same as that obtained from the gel-healing process.[20]

3.4. Small-Angle Neutron Scattering (SANS). Figure 11a shows the concentration variations of SANS intensity functions, $I(q)$s, for **1-Cl**/water at 25 °C. Here, incoherent scattering correction was made for both the gelator and the solvent. This figure shows that $I(q)$s are monotonically decreasing functions of q and increase with increasing **1-Cl** concentration, C. A similar SANS behavior was obtained in other gelators carrying

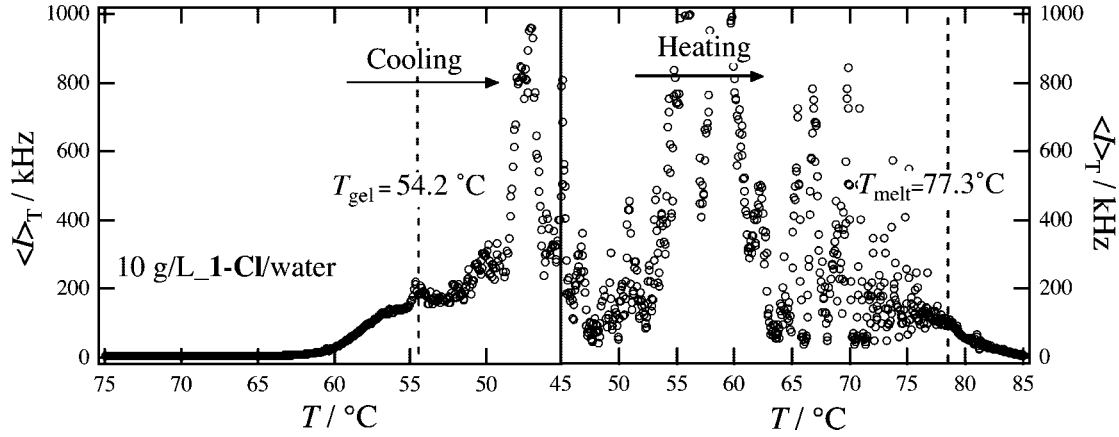

Figure 8. Variations of the scattering intensity with temperature during cooling and heating processes for 10 g/L **1-Cl**/water.

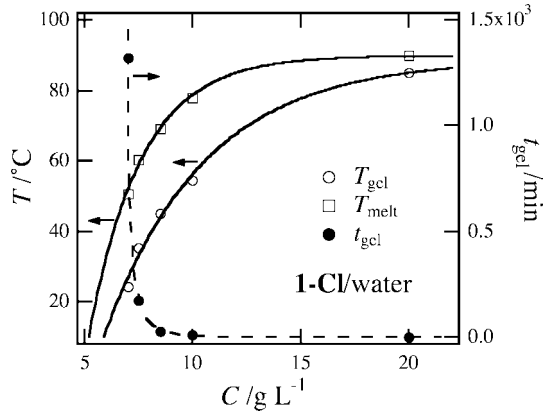

Figure 9. Variations of the gelation temperature, the gel melting temperature, and the gelation time with concentration, *C*. The solid curves are the exponential fitting curves, and the dashed curve is drawn as a guide for the eye.

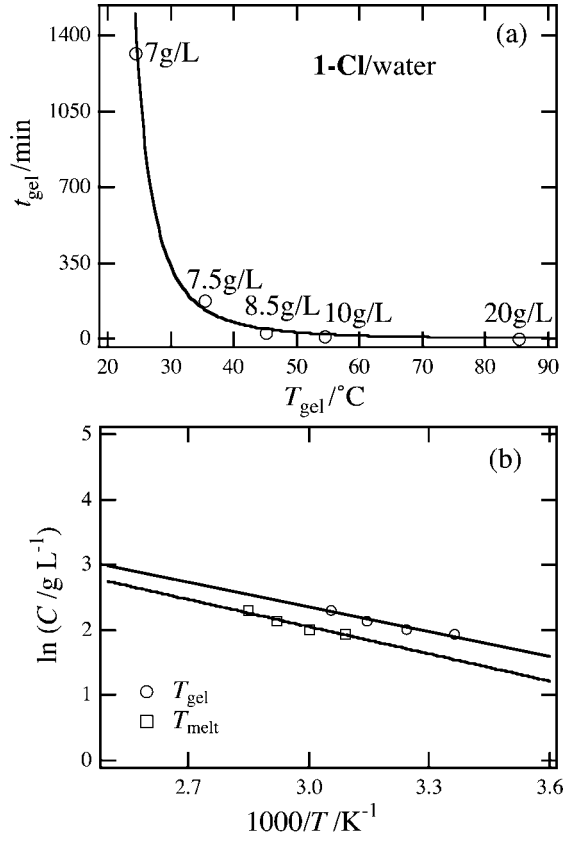

Figure 10. (a) Time−temperature phase diagram and (b) dependence of the reciprocal gelation and gel-melting temperatures on ln *C*. The evaluated values of T_c and α are respectively, 17.1 °C and 2.8.

amide group, ureylene group, siloxane groups, etc.[44,45] *I*(*q*)s could be superimposed by normalizing with the gelator concentrations, indicating self-similar structure of gels irrespective of the concentration.

Figure 11b shows the normalized scattering functions divided by **1-Cl** concentration, *C*. It is seen from this figure that *I*(*q*)s are not superimposed by normalizing with the gelator concentration. It indicates that *I*(*q*)s are strongly concentration dependent. It is also supported by the concentration dependence of the fitting parameters (Figure 7) obtained from eq 9. It has been disclosed in the previous report[20] that H-bonding between the amide groups of **1-Cl** molecules takes place via chloride ions and with water molecules. There is also a large probability to make network formation by C═O group of **1-Cl** molecules via chlorine ions and with water molecules that might cause of the concentration dependence of *I*(*q*).

Figure 12 shows the temperature variations of the scattering intensity functions, *I*(*q*), by light scattering ($q < 0.003$ Å^{-1}) and by SANS (0.003 Å$^{-1} < q$) for (a) 10 g/L **1-Cl**/water and (b) 20 g/L **1-Cl**/water. It is seen from Figure 12a,b that *I*(*q*)s change systematically with temperature. The scattering intensity can be expressed as

$$I(q) = n_p P(q)\, S(q) \qquad (12)$$

where n_p is the number density of particles and *P*(*q*) is the single particle scattering function. *S*(*q*) is the structure factor for the dispersion that describes pair correlations between particles, and it holds as long as there is no correlation between the relative locations of particles and their respective orientations. It was discussed before from light-scattering study that **1-Cl** hydrogel forms a rodlike assembly. If they take random orientations, the single-particle scattering function can be calculated as an average over all orientations

$$P(q) \sim \int_{\gamma=0}^{\pi/2} \frac{\sin^2(qH\cos\gamma)}{(qH\cos\gamma)^2} \frac{J_1^2(qR\sin\gamma)}{(qR\sin\gamma)^2} \sin\gamma\, d\gamma \qquad (13)$$

where $J_1(x)$ is the Bessel function of order 1, γ is the angle between the preferential axis of the cylinder and **q**, and 2*H* and 2*R* are the length and diameter of the rod, respectively. For

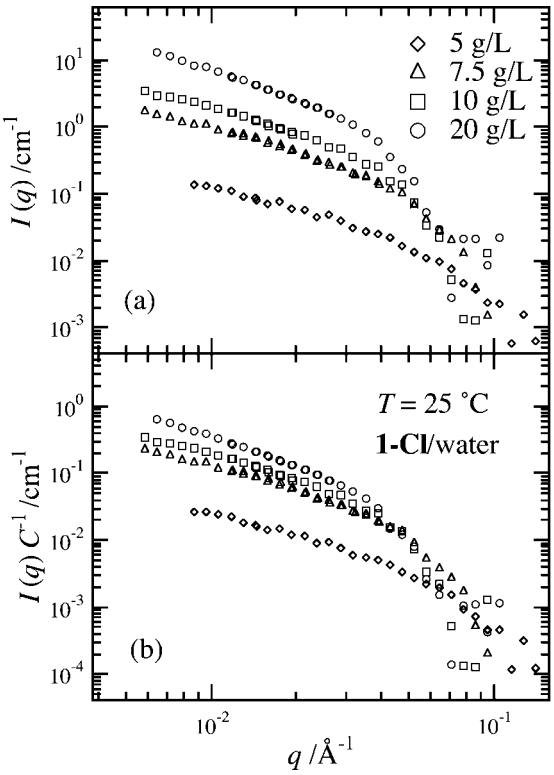

Figure 11. Concentration variations of the (a) SANS scattering functions and (b) normalized SANS scattering functions divided by the concentration, C, for **1-Cl**/water at 25 °C.

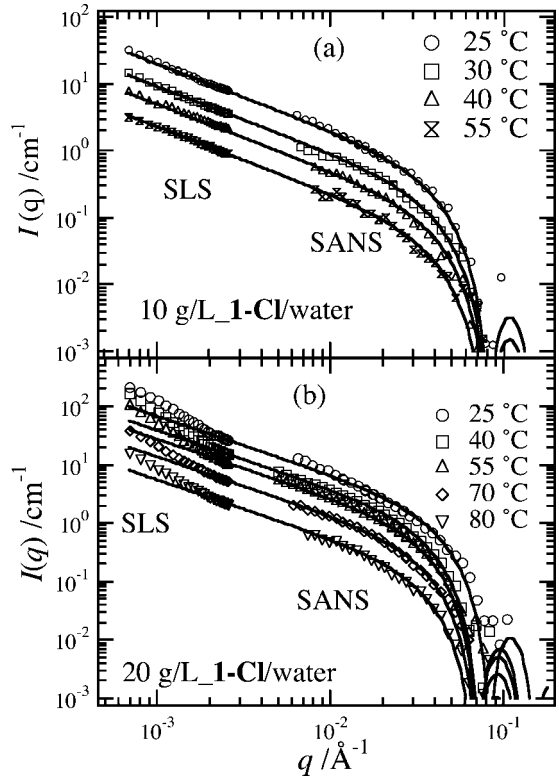

Figure 12. Temperature variations of the SANS and SLS scattering intensity functions for (a) 10 g/L **1-Cl**/water and (b) 20 g/L **1-Cl**/water.

randomly oriented rods with a large aspect ratio, $H \gg R$, eq 13 can be approximated to the following equation:[47]

$$P(q) \sim \frac{1}{q}\left[\frac{J_1(qR)}{qR}\right]^2 \qquad (14)$$

Hence, the asymptotic behavior at low q is q^{-1}. The **1-Cl** hydrogel well obeys the $I(q) \sim q^{-1}$ behavior given by eq 14. The initial slope is very close to -1, and the slope changes at around $q = 0.03$ Å^{-1}. It is seen from Figure 12a that both SLS and SANS intensity functions are well represented by eq 14 for all temperatures. It is also seen from Figure 12b that both SLS and SANS intensity functions in the high q region are well represented by eq 14 for all temperatures. But, below $q = 0.002$ Å^{-1}, the experimental data points are above the $P(q)$ curves for all temperatures. According to eq 12, this upward trend is caused by the interparticle interferences. The corresponding structure factor $S(q)$ is also shown in Figure 13 as a function of ($q \times 2R$) for (a) 10 g/L **1-Cl**/water and (b) 20 g/L **1-Cl**/water. It is seen from Figure 13a that for 10 g/L **1-Cl**/water, $S(q) \approx 1$ for all temperatures. It indicates that there is no correlation between the relative locations of particles and their respective orientations. Figure 13b shows that for 20 g/L **1-Cl**/water, $S(q)$ is almost unity at high q values. At low q values, there is a strong upturn originating from interparticle interference[48] that correlates the relative locations of particles with their respective orientations. This figure also shows that $S(q)$ decreases with increasing temperature. However, the diameter of the rod is easily obtained by using eq 14. Figure 14 shows the temperature dependence of the diameter of the rod obtained from 10 and 20 g/L **1-Cl**/water using eq 14. It is seen from this figure that the diameter of the rod is almost temperature independent but concentration dependent and its

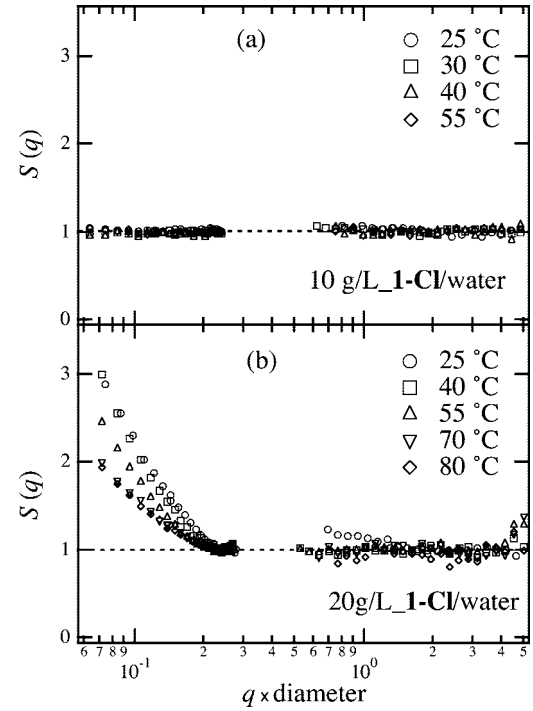

Figure 13. Temperature variations of the structure factor, $S(q)$, as a function of ($q \times 2R$) for (a) 10 g/L **1-Cl**/water and (b) 20 g/L **1-Cl**/water.

value is obtained to be 9.3 and 10.5 nm for 10 and 20 g/L **1-Cl**/water, respectively. Note that detailed description of the polydispersity of the cross section was intensively examined by Guenet.[49] According to his work, smearing by polydispersity and transitional **q** region appear before the so-called Porod low region is entered, depending on the lower and

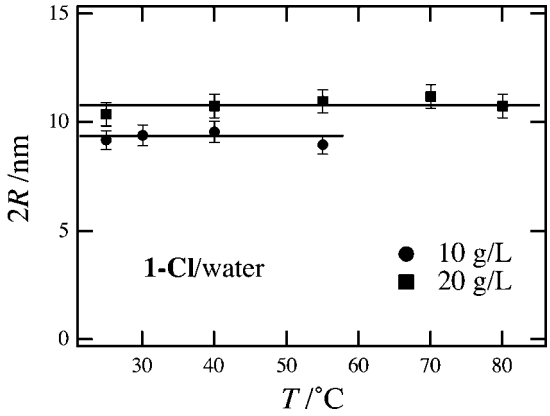

Figure 14. Temperature-dependent diameter of the randomly oriented rods determined from eq 14. Error bar shows standard deviation. The solid lines are the linear fitting lines.

upper cutoffs of the rod cross sections. In the present system, it is very difficult to estimate the length of the rod because of the lack of cutoff information. However, we can calculate the length of the rod using the following equation

$$R_g^2 = \frac{(2H)^2}{12} + \frac{(2R)^2}{8} \qquad (15)$$

where R_g is the radius of gyration. If we consider $R_g \approx 35.7$ nm, that obtained from SLS, the length ($2H$) of the rod is calculated to be approximately around 120 nm both for 10 and 20 g/L **1-Cl**/water. Similar rodlike structures were obtained by Okabe et al.[46] from the organogels.

4. Conclusion

The structure and the gelation kinetics of hydrogel consisting of an oligomeric electrolyte, **1-Cl,** were investigated by means of SLS/DLS and SANS. We successfully obtained the values of weight-average molecular weight ($M_w \approx 5.12 \times 10^3$ Da), radius of gyration ($R_g \approx 35.7$ nm), second virial coefficient ($A_2 \approx 7.88 \times 10^{-5}$ mol cm^3/g^2), and hydrodynamic radius ($\langle R_h \rangle_{av} \approx 22.4$ nm) from the SLS/DLS measurements on the dilute aqueous solutions of **1-Cl** far below the gelation threshold. We also estimated the degree of polymerization to be ca. 22.

In the sol state, ICF indicated two modes: the translational diffusion mode (fast mode) and the stretched exponential mode (slow mode). ICF entailed a power law behavior at the sol−gel transition and the value of the fractal exponent (n) evaluated to be 0.6. The fractal exponent (n) was almost concentration independent whereas the fraction of the translational diffusion mode (A) and the characteristic time (τ^*) were concentration dependent irrespective of t_{gel}, T_{gel}, and T_{melt}. The gel point was also clearly observed as the deviation of the intensity of ICF. **1-Cl** exhibited a large hysteresis loop during a temperature cycle. The threshold temperature (17.1 °C) and the critical concentration of gelation (6.3 g/L) were well obtained by DLS. The power law exponent, α (=2.8), obtained from the time (t_{gel})−temperature (T_{gel}) phase diagram was close to the fractal dimension, D (=3). The concentration-dependent gelation and gel melting temperatures followed the van't Hoff equation, and the enthalpy of cross-link formation was estimated to be ca. −10 kJ/mol.

1-Cl showed that the unit structure of the gel was strongly concentration dependent. SANS experiments revealed that the unit structure of the gel network has rodlike assemblies, which was indicated by the R_g/R_h ratio from SLS study. The gel consisted of rodlike elements aggregated to each other. The diameter of the rod was concentration dependent (9.3 nm for 10 g/L **1-Cl**/water and 10.5 nm for 20 g/L **1-Cl**/water), and the length of the rod was calculated to be approximately 120 nm for both 10 and 20 g/L **1-Cl**/water. The fractal behavior was observed for 20 g/L **1-Cl**/water and indicated the correlation between the relative locations of particles and their respective orientations.

Acknowledgment. This work was partly supported by the Ministry of Education, Science, Sports and Culture, Japan, for Scientific Research on Priority Areas, 2006-2010, No. 18068004, and the Industrial Technology Research Grant Program (05A25710a) from the New Energy and Industrial Technology Development Organization.

References and Notes

(1) Bohidar, H. B.; Dubin, P.; Osada, Y. *Polymer Gels: Fundamentals and Applications*; American Chemical Society: Washington, DC, 2003.
(2) Rossi, D.; Kajiwara, K.; Osada, Y.; Yamauchi, A. *Polymer Gels*; Plenum: New York, 1991.
(3) Brenzinger, K. *Z. Physiol. Chem.* **1892**, *16*, 552.
(4) Estroff, L. A.; Hamilton, A. D. *Chem. Rev.* **2004**, *104*, 1201.
(5) Lee, K. Y.; Mooney, D. J. *Chem. Rev.* **2001**, *101*, 1869.
(6) Hanabusa, K.; Hiratsuka, K.; Kimura, M.; Shirai, H. *Chem. Mater.* **1999**, *11*, 649.
(7) Nakashima, T.; Kimizuka, N. *Adv. Mater.* **2002**, *14*, 1113.
(8) Vinogradov, S. V.; Bronich, T. K.; Kabanov, A. V. *Adv. Drug Delivery Rev.* **2002**, *54*, 135.
(9) John, G.; Vemula, P. K. *Soft Matter* **2006**, *2*, 909.
(10) Bieser, A. M.; Tiller, J. C. **2005**, *Chem. Commun.* (31) 3942.
(11) Shome, A.; Debnath, S.; Das, P. K. *Langmuir* **2008**, *24*, 4280.
(12) Trivedi, D. R.; Ballabh, A.; Dastidar, P. *J. Mater. Chem.* **2005**, *15*, 2606.
(13) Schmidt, R.; Adam, F. B.; Michel, M.; Schmutz, M.; Decher, G.; Mesini, P. J. *Tetrahedron Lett.* **2003**, *44*, 3171.
(14) Shirakawa, M.; Fujita, N.; Shinkai, S. *J. Am. Chem. Soc.* **2005**, *127*, 4164.
(15) Abdallah, D. J.; Weiss, R. G. *Adv. Mater.* **2000**, *12*, 1237.
(16) Moniruzzaman, M.; Sundararajan, P. R. *Langmuir* **2005**, *21*, 3802.
(17) George, M.; Snyder, S. L.; Terech, P.; Glinka, C. J.; Weiss, R. G. *J. Am. Chem. Soc.* **2003**, *125*, 10275.
(18) Mohmeyer, N.; Schmidt, H. W. *Chem. Eur. J.* **2005**, *11*, 863.
(19) Bhuniya, S.; Park, S. M.; Kim, B. H. *Org. Lett.* **2005**, *7*, 1741.
(20) Kundu, S. K.; Matsunaga, T.; Yoshida, M.; Shibayama, M. *J. Phys. Chem. B* **2008**, *112*, 11537.
(21) Yoshida, M.; Koumura, N.; Misawa, Y.; Tamaoki, N.; Matsumoto, H.; Kawanami, H.; Kazaoui, S.; Minami, N. *J. Am. Chem. Soc.* **2007**, *129*, 11039.
(22) Pike, E. R.; Pomeroy, W. R. M.; Vaughan, J. M. *J. Chem. Phys.* **1975**, *62*, 3188.
(23) Burchard, W. *Adv. Polym. Sci.* **1983**, *48*, 85.
(24) Mrkvickova, L.; Porsch, B.; Sundelof, L.-O. *J. Appl. Polym. Sci.* **1995**, *58*, 2033.
(25) Wittgren, B.; Borgstrom, J.; Piculell, L.; Wahlund, K.-G. *Biopolym.* **1998**, *45*, 85.
(26) Viebke, C.; Williams, P. A. *Food Hydrocolloids* **2000**, *14*, 265.
(27) Shibayama, M.; Takata, S.; Norisuye, T. *Physica A* **1998**, *249*, 245.
(28) Shibayama, M.; Norisuye, T. *Bull. Chem. Soc. Jpn.* **2002**, *75*, 641.
(29) Shibayama, M. *Bull. Chem. Soc. Jpn.* **2006**, *79*, 1799.
(30) Hashimoto, T.; Kowsaka, K.; Shibayama, M.; Suehiro, S. *Macromolecules* **1986**, *19*, 750.
(31) Martin, J. E.; Wilcoxon, J. *Phys. Rev. Lett.* **1988**, *61*, 373.
(32) Ren, S. Z.; Shi, W. F.; Zhang, W. B.; Sorensen, C. M. *Phys. Rev. A* **1992**, *45*, 2416.
(33) Nystrom, B.; Roots, J.; Carlsson, A.; Lindman, B. *Polymer* **1992**, *33*, 2875.
(34) Martin, J. E.; Wilcoxon, J.; Odinek, J. *Phys. Rev. A* **1991**, *43*, 858.
(35) Winter, H. H.; Chambon, F. *J. Rheol.* **1986**, *30*, 367.
(36) Durand, D.; Delsanti, M.; Adam, M.; Luck, J. M. *Europhys. Lett.* **1987**, *3*, 297.
(37) Matsunaga, T.; Shibayama, M. *Phys. Rev. E, Rapid. Commun.* **2007**, *76*, 030401.
(38) Pusey, P. N.; van Megen, W. *Physica A* **1989**, *157*, 705.
(39) Norisuye, T.; Shibayama, M.; Nomura, S. *Polymer* **1998**, *39*, 2769.
(40) Muthukumar, M. *Macromolecules* **1989**, *22*, 4656.

(41) Muthukumar, M. *J. Chem. Phys.* **1985**, *83*, 3161.
(42) Martin, J. E.; Adolf, D.; Wilcoxon, J. P. *Phys. Rev. A* **1989**, *39*, 1325.
(43) Nowak, A. P.; Breedveld, V.; Pakstis, L.; Ozbas, B.; Pine, D. J.; Pochan, D.; Deming, T. J. *Nature* **2002**, *417*, 424.
(44) Breedveld, V.; Nowak, A. P.; Sato, J.; Deming, T. J.; Pine, D. J. *Macromolecules* **2004**, *37*, 3943.
(45) Okabe, S.; Ando, K.; Hanabusa, K.; Shibayama, M. *J. Polym. Sci., Part B, Polym. Phys. Ed.* **2004**, *42*, 1841.
(46) Okabe, S.; Hanabusa, K.; Shibayama, M. *J. Polym. Sci. Part B, Polym. Phys. Ed.* **2005**, *43*, 3567.
(47) Shibayama, M.; Nomura, S.; Hashimoto, T.; Thomas, E. L. *J. Appl. Phys.* **1989**, *66*, 4188.
(48) Huang, J. S.; Safran, S. A.; Kim, M. W.; Grest, G. S.; Kotlarchyk, M.; Quirke, N. *Phys. Rev. Lett.* **1984**, *53*, 592.
(49) Guenet, J. M. *J. Phys. II Fr.* **1994**, *4*, 1077.

JP807992T